

Landscape appreciation of systematic structure properties in even-even nuclei along the valley of stability

Hai-Yan Meng and Hua-Lei Wang*

School of Physics and Microelectronics, Zhengzhou University, Zhengzhou 450001, China

Min-Liang Liu

*Key Laboratory of High Precision Nuclear Spectroscopy, Institute of Modern Physics,
Chinese Academy of Sciences, Lanzhou 730000, China and*

School of Nuclear Science and Technology, University of Chinese Academy of Sciences, Beijing 100049, China

Structural properties of even-even nuclei along the β -stability line are systematically analyzed and investigated by means of our improved potential-energy-surface (PES) approach. The equilibrium deformations obtained from the PES minima are compared with available experimental data and other theoretical results. From a brand-new angle of view, taking the nuclei on the stability line as footholds, we systematically present two-nucleon separation energies and half lives in the corresponding isotopic chains. Very regular laws can be seen, especially below $Z = 84$. The observed trends and anomalous behaviors are briefly discussed. The energy difference between theory and experiment for the binding energies and two-nucleon separation energies indicates that the improved PES calculations with our fitting macroscopic model parameters are relatively in better agreement with experiments. Based on the systematic law of two-nucleon separation energies, the bound limit of even-even nuclei is crudely estimated along the stability line.

PACS numbers: 21.10.Re, 21.60.Cs, 21.60.Ev

I. INTRODUCTION

Most of the nuclei in nature were formed at the creation of the universe or after supernovae explosions [1]. Their half-lives are usually longer than the expected age of the Earth and the Solar System (~ 4.6 billion years) or the Universe (~ 13.8 billion years), indicating they are stable or practically stable. These stable nuclei, less than 300 nuclides (the nuclide number is slightly different, depending on time scale used), form a ‘valley of stability’ (which is also referred as ‘belt of stability’ or ‘band of stability’, or a ‘peninsula of stability’ in a ‘sea of instability’) in the nuclear chart. The nuclei in the valley are of special interest in nuclear physics because they are not only naturally existent but also the important candidates of the projectile-target combinations in nuclear reactions used for producing radioactive nuclei though the high-intensity radioactive beam facilities and the radioactive targets start to be used nowadays [2].

Along the valley of stability, the semi-empirical approximation formulas were fitted half a century ago, such as $N - Z = 0.4A^2/(A + 200)$ in Ref. [3] and $Z = A/(1.98 + 0.0155A^{2/3})$ in Ref. [4], which can allow one to estimate the mass number, A , or neutron number, N , for a given proton number, Z . The curves described by such two formulas are usually referred to as the β -stability lines (also, the backbone of the belt of stability) and almost overlap except for the slightly different extrapolations in the high- Z region. The nuclei located at the northwest (southeast) of the stability line contain too

many protons (neutrons) to be stable, tending to become stable ones by, e.g., α -, β^- -, β^+ -decay or electron capture and allowing them to move closer to the optimal neutron-proton ratio. As is well known, only certain number of combinations of neutrons and protons can form the stable nucleus which has enough ability (e.g., binding energy) to permanently hold its nucleons together (however, regardless of neutron-proton combinations, no stable members are identified in some isotopes with $Z > 83$). It has been found that the nuclei consisting of specific nucleon numbers, e.g., 2, 8, 20, 28, 50, 82 and 126 (for neutrons), have prominent stability, possessing a relatively higher average binding energy per nucleon. Such magic numbers corresponding to shell closures have been predicted by the nuclear shell-structure model [5–9] and proved by experimental observables with sudden discontinuities [10], e.g., in the nucleon separation energies with changing Z or N .

Up to now, the heaviest doubly magic nucleus is $^{208}_{82}\text{Pb}_{126}$, almost lying on the stability line. Naturally, the search for next heavier doubly magic nucleus and the northeast limit of the nuclear chart is more fascinating. Theoretical models based on the macroscopic-microscopic approaches [11–20] using various potentials predicted that the heavier doubly magic candidate is the superheavy nucleus $^{298}_{114}\text{Fl}_{184}$, which lies very closely to this extrapolated β -stability line and may be stable enough to exist in nature. Some self-consistent mean-field calculations prefer $Z = 120$ and $N = 172$ to be the shell closures [20–23]. Furthermore, around the next doubly magic nucleus, the predictions also show that there may exist a batch of shell-stabilized superheavy nuclei which form a small so-called “island of stability” (relative to the “peninsula of stability”). It is expected that nuclei

* wanghualai@zzu.edu.cn

near the top of the island of stability can exist for, e.g., many years instead of some milliseconds [24]. Presently, along the stability line, the experimentally synthesized heaviest even-even nucleus is the nucleus $^{264}_{102}\text{No}_{162}$ [25] though the periodic table of elements has contained 118 known and named elements [26–29].

As mentioned above, nuclear structural properties will strongly affect the stability of nuclei. Nuclear binding energies and decay half-lives increase markedly in the vicinity of nucleon closed shells which give rise to spherical nuclear shapes. Indeed, nuclear shape is very helpful for understanding the fundamental interaction related to microscopic nuclear structure. It is known that nuclear stability both in the superheavy and drip-line regions depends on nuclear deformations. For instance, the fission barriers and the nucleon(s) separation energies are to a large extent related to ground-state nuclear deformations. Theoretically, these low-lying nuclear structure phenomena can be well described by the mean field approach. Though the self-consistent Hartree-Fock or relativistic mean-field microscopic theories have been well developed during the past several decades, the well-known Nilsson or Woods-Saxon (WS) one-body mean-field potentials are still widely used in nuclear structure research and never stop developing. We have conducted some related studies [30–36] by using the PES calculation method within the framework of the macroscopic-microscopic models.

The present investigation focusing on the ground-state properties (e.g., shapes and binding energies) of even-even nuclei along the valley of stability up to the predicted superheavy island (near the $^{298}_{114}\text{Fl}_{184}$ nucleus) are performed in term of the realistic WS potential (a good approximation of the self-consistent Hartree-Fock mean-field), combining two different macroscopic and microscopic parts. Such an empirical potential poses a high predictive power while its computing algorithms are relatively simple. Very recently, we performed the investigation of the propagating uncertainties from the WS potential parameters [36]. However, the single-particle mean field is not of our primary concern here, from the point of view of model the main contribution of the present work is to provide a set of new macroscopic-model parameters by the least-square fitting to recently experimental data [10]. In addition, from the special footholds, we exhibit and analyze the experimental half-lives and two-nucleon separation energies of available even-even nuclei. With the improved PES method, we evaluate the even-even nuclei up to the predicted “island of superheavy elements” along the β –stability line. A crudely bound limit based on two-nucleon separation energies is proposed by an empirical extrapolation which does not include any interaction assumption.

The paper is organized as follows. In Sec. II, we briefly introduce the unified procedure of two potential energy surface methods used and simultaneously provide the necessary references. The results and discussions are presented in Sec. III. At last, we give a summary in Sec.

IV.

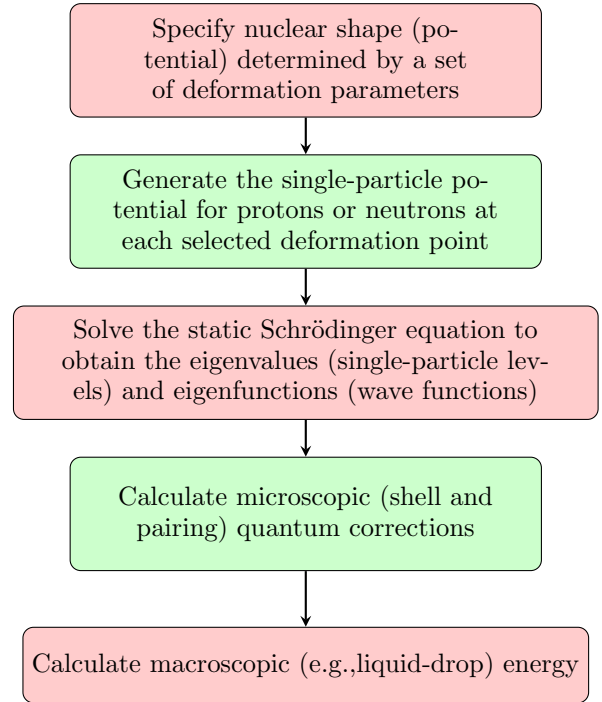
II. THEORETICAL FRAMEWORK

A. General description of PES method

For a long time many results have been obtained by the PES method with the realistic WS potential. A short presentation of the unified procedure of this treatment will be given below, including the necessary references. The basic idea in this approach is that the total binding energy of a nucleus can usually be decomposed in two parts,

$$E_{\text{total}}(Z, N, \beta) = E_{\text{mac}}(Z, N, \beta) + E_{\text{mic}}(Z, N, \beta) \quad (1)$$

where E_{mac} is the macroscopic bulk-energy term, being a smooth function of Z , N and/or deformation, and E_{mic} is the microscopic quantum corrections calculated, e.g., from a phenomenological single-particle potential well. β denotes a set of deformation coordinates in the deformation space (β_2, γ, β_4). In general, the calculated procedure is carried out in five steps, e.g., as mentioned in Ref. [37]:



The total potential energy can obviously be given by the sum of macroscopic and microscopic energies obtained in the last two steps. Some different variants of the PES method have been developed according to the different ways of treating these five steps.

In this work, we describe the nuclear shape by means of the parametrization of the nuclear surface with the help of spherical harmonics. The nuclear potential is calculated in a multi-dimensional space (β_2, γ, β_4) including

the axial and non-axial deformation degrees of freedom. The single-particle energies (eigenvalues) and the corresponding wave functions (eigenfunctions) are obtained by solving the static Schrödinger equation with a WS-type nuclear potential, including a central potential, a spin-orbit coupling potential and the Coulomb potential for the protons (e.g., see Sec. 2 in Ref. [38] for detailed expressions). That is, by giving a set of the WS parameters (e.g., the Universal parameter set is adopted here; see Table 1 in Ref. [38]), the deformed WS potential can be generated numerically at each $(\beta_2, \gamma, \beta_4)$ deformation lattice. The WS Hamiltonian matrix elements are calculated by using the basis of the axially deformed harmonic oscillator in the cylindrical coordinate system. Then the single-particle solutions (e.g., levels and wave functions) are given by diagonalizing the Hamiltonian matrix. Next, by using the single-particle levels obtained, the shell and pairing corrections at each deformation point $(\beta_2, \gamma, \beta_4)$ are respectively calculated in terms of the Strutinsky method [39] and Lipkin-Nogami (LN) method [40]. It is worth noting that the LN method allows avoiding the spurious pairing phase transition which may occur in the calculation of the traditional Bardeen-Cooper-Schrieffer (BCS) type. The monopole pairing is taken into account and its strength, G , is estimated by the average gap method [41]. The adopted pairing windows for both protons and neutrons contain dozens of single-particle levels, e.g., half of the particle number Z and N , below and above the Fermi surface.

The macroscopic energy is usually calculated by the liquid drop (LD) model. Nowadays, there exist many phenomenological LD models in the literatures. Below, we list several frequently used ones in the macroscopic-microscopic calculations, such as the standard LD model [42], the finite-range droplet model [43], the Lublin-Strasbourg drop model [44], etc. These macroscopic models with slightly different properties are usually used for calculating the smoothly varying part of the nuclear energy, in which the dominating terms are associated with the volume energy, the surface energy, the symmetry energy and the Coulomb energy.

B. Two variants of PES calculations

In the present work, we perform the calculation for the total binding energy (defined as negative) by two PES methods with slightly different treatments in macroscopic and microscopic energies. In the first method, the macroscopic energy E_{LD1} is calculated by a standard LD model [42], namely,

$$E_{LD1}(N, Z, \beta) = a_1 \left[1 - \kappa \left(\frac{N-Z}{A} \right)^2 \right] A + a_2 \left[1 - \kappa \left(\frac{N-Z}{A} \right)^2 \right] A^{2/3} B_S + c_3 \frac{Z^2}{A^{1/3}} B_C + c_4 \frac{Z^2}{A}, \quad (2)$$

where the model parameters $a_1 = -15.677$ MeV, $a_2 = 18.56$ MeV, $c_3 = 0.717$ MeV, $c_4 = -1.2113$ MeV, and $\kappa = 1.79$. The relative surface and Coulomb energies B_S and B_C are only functions of nuclear shape. The shell and pairing corrections are considered in the microscopic energy E_{mic1} which reads [39],

$$E_{mic1}(Z, N, \beta) = E_{shell}(Z, N, \beta) + E_{pair}(Z, N, \beta). \quad (3)$$

Note that the treatments for the microscopic corrections can be found in Refs. [39, 40] (also, cf. Refs. [30–35] and references therein). Since these are widely used and relatively standard, it is not necessary to give the detailed description here. As described above, the total binding energy (in order to compare with data, the absolute value is used here) of a nucleus can be calculated by summing the macroscopic and microscopic energies at each deformation grid. The smoothed PES can finally be obtained by interpolating, e.g., using a spline function, between the calculated sampling points. The nuclear properties including the equilibrium deformations, binding energies, and so on can be analyzed already with the help of the minima of the PES. For short, we call this method PES-1 in this work.

Now let us introduce the second PES calculation which is similarly referred to as PES-2 below. In this method, the corresponding macroscopic energy is given by [45, 46],

$$E_{LD2}(N, Z) = a_v A + a_s A^{2/3} + \frac{a_{sym} T(T+1)}{A} + \frac{a_{asym} T(T+1)}{A^{4/3}} + C \frac{Z^2}{A^{1/3}} + C_4 \frac{Z^2}{A}. \quad (4)$$

Note that the present coefficients of Eq.(4) are obtained by us through a least-square fit to the binding energies of available 578 even-even nuclei [10]. During the parameter fit, the χ^2 function is defined as

$$\chi^2 = \sum_{i=1}^{578} (B_i^{\exp} - B_i^{\text{theo}})^2, \quad (5)$$

where B_i^{theo} stands for the calculated binding energy (namely, the negative E_{total} as mentioned above) and B_i^{\exp} for experimental data.

Table I shows the old [46] and new (present) parameters for the LD energy defined in Eq.(4), together with their root-mean-square (rms) deviation values (characterizing to some extent the quality of the fit). It should be pointed out that the rms value given by PES-1 is 4.505 MeV, which is greater than those values obtained by PES-2 (e.g., 0.667 or 0.614 MeV, as seen in Table I). At this time, the microscopic part is defined as (same to that in Ref. [46])

$$E_{mic2}(Z, N, \beta) = E_{def}(Z, N, \beta) + E_{shell}(Z, N, \beta) + E_{pair}(Z, N, \beta), \quad (6)$$

where the shell and pairing corrections E_{shell} and E_{pair} are same to those in Eq.(3). The deformation correction

TABLE I. Two sets of parameters of the macroscopic LD energy E_{LD2} [45, 46], as defined in Eq.(4). Note that the old parameters are taken from [46] and the new ones are refitted to 578 even-even nuclei in the AME2016 mass table. Two rms values are calculated for these 578 even-even nuclei based on the old and new parameters, respectively. Energies are in units of MeV.

	a_v	a_s	a_{sym}	a_{asym}	C	C_4	σ_{rms}
Old	-15.707	18.302	117.481	-161.323	0.717	-0.882	0.667
New	-15.725	18.403	118.228	-165.496	0.719	-0.919	0.614

energy is written as [38, 42, 47]

$$E_{\text{def}}(Z, N, \beta) = \left\{ \left[B_S(\beta) - 1 \right] + 2\chi \left[B_C(\beta) - 1 \right] \right\} E_S^{(0)}, \quad (7)$$

where the spherical surface energy $E_s^{(0)}$ and the fissility parameter χ are Z - and N -dependent, cf. Refs. [42, 47]. The quantities B_S and B_C are same to those in Eq.(2) which includes the deformation energy. The summation of two terms E_{LD2} and $E_{\text{mic}2}$ gives the total binding energy in the PES-2 calculation.

Note that the PES-1 and PES-2 calculations will give the same equilibrium deformations but different binding energies since the treatments of the deformation energy, shell and pairing corrections are same but the spherical LD energies different. With the aid of the PES calculations, the present work will investigate some nuclear properties associated with the shape and binding energies along the β -stability line. In addition, Xu et al [48] performed the configuration-constrained PES calculation for the high- K isomers where the binding energy calculated by the PES-1 method was used for adjusting the pairing strength based on the five-point mass formula [41]. Such an adjustment is of importance for reproducing the excitation energies of high- K states. Relative to PES-1 calculation, the present improvement reduced the rms value of the binding energies for 578 even-even nuclei from 4.505 to 0.614 MeV. It will be reasonable to believe that the improved PES calculation will give a better description for the adjustment of the pairing strength since it can provide the relatively accurate binding energy (but this is beyond our present project and we just focus on even-even nuclei here).

III. RESULTS AND DISCUSSION

In order to evaluate the nuclear properties, some phenomenological or empirical or systematic laws are often used since they are usually simple but valid and weakly model-dependent, even model-independent. As is pointed out by Casten et al. [49], the P ($P \equiv$

$N_p N_n / (N_p + N_n)$) factor is one of the phenomenological quantities where N_p and N_n are respectively the numbers of valence protons and neutrons (for more details, e.g., cf. Refs. [49–53]). Nuclear collectivity and deformation, especially in the heavy nuclei region, are expected to depend on it sensitively. As is known, nuclear deformation depends to an extent on the competition between the like-nucleon pairing interaction and the neutron-proton interaction [49]. Such competition can be suitably described by the P factor defined above since it can be viewed as the average number of interactions of each valence nucleon with those of the other type. Much empirical evidence [52] indicates that n-p residual interaction and the pairing gap are typically on the order of 250 keV and 1.0-1.5 MeV, respectively. When each valence nucleon interacts with about 4-5 nucleons of the other type (corresponding to $P \sim 4 - 5$), the transition to deformation will occur near this domain. At that time, the residual n-p and pairing interactions become competitive. Using the contour maps of the P factor as the background, Figure 1 illustrates the available stable nuclei and the β -stability lines plotted in terms of the formulas $N - Z = 0.4A^2/(A + 200)$ [3] and $Z = A/(1.98 + 0.0155A^{2/3})$ [4], together with the predicted drip-lines [18] and the boundaries of even-even nuclei synthesized experimentally. One can evaluate the P -factor distribution along the stability line. We can notice that the stability lines almost go across the top of the highest P -factor ‘hill’. Near this ‘peak’, the rotational bands are identified in ^{254}No [54] and ^{256}Rf [55, 56], indicating the expected collectivity and deformed properties.

In this paper, we choose to investigate the nuclear properties of 59 even-even nuclei which lie on or are the closest to the β -stability line (the Green’s expression [3], $N - Z = 0.4A^2/(A + 200)$, is arbitrarily adopted) for given even proton numbers from $Z = 2$ to 118. Of course there will be 88 even-even nuclei on the stability line for given even neutron numbers from $N=2$ to 176 (the largest N in the observed even-even nuclei), but the obtained conclusions will be similar. As shown in Fig. 2(a), the plot of the P -factor as a function of Z indicates there are two peaks which are higher than the critical shadow region. To cross-check this large collective behaviour, we present the $R_{4/2}$ ($\equiv E(4_1^+)/E(2_1^+)$) ratio of the selected 55 even-even nuclei in Fig. 2(b), together with several critical points (see Refs. [58–66] for more details). Such a parameter is arguably one of the the best indicators of changes in low-lying nuclear structure. Though it cannot describe the magnitude of the deformation, it is often able to provide nuclear deformed properties [67]. Moreover, these critical $R_{4/2}$ values are widely used to identify collective properties of even-even nuclei. Figure 2(b) illustrates most of nuclei on the stability line exhibit the collective behaviour with $R_{4/2} > 1.82$ (the Mallmann critical point [58]), in good agreement with the results given by the P -factor plot.

Figure 3 shows the ground-state equilibrium deforma-

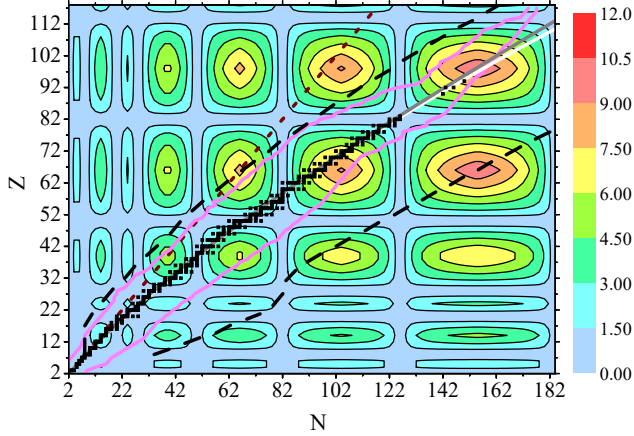


FIG. 1. (Color online) Valley of stability and several typical boundaries on $Z - N$ plane, using the P -factor contour map as the background. The black square symbol corresponds to a stable nucleus which is arbitrarily defined as one with a half-life longer than $\sim 10^8$ years. In such a classification, there will be 288 nuclides in total [1]. The gray and white solid lines represent the two stability lines calculated by using the formula given in Ref. [4] and Ref. [3], respectively. The region between the two pink solid lines denote the nuclei have already been observed or synthesized [25]. The two black long-dash lines above and below the valley of stability respectively indicate the proton and neutron drip lines given by Möller et al. [57]. The wine short-dash line is the $N = Z$ line, just using to guide the eye.

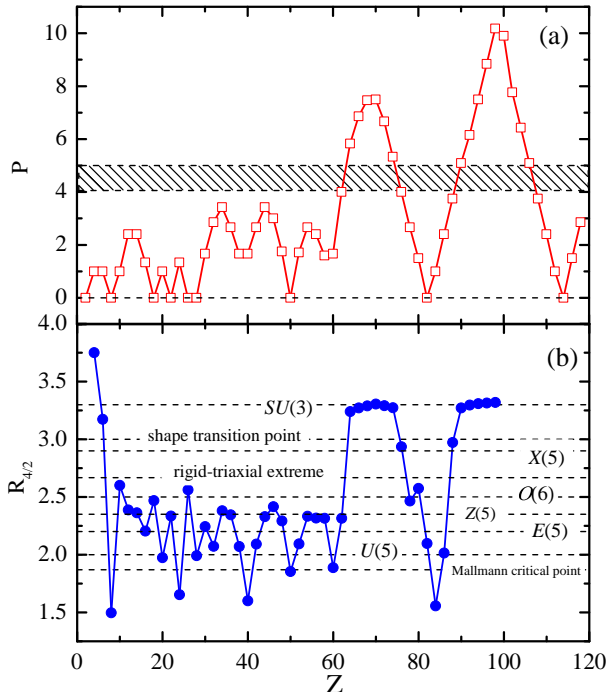


FIG. 2. (Color online) The available phenomenological quantities $R_{4/2}$ ratio [25] (a), P factor (b) for even-even nuclei along the β -stability line.

tions β_2 , γ and β_4 obtained from the calculated PES minima for even-even nuclei along the stability line, together with the calculations by the folded-Yukawa (FY) single-particle potential and the finite-range droplet model (FRDM) [57] and the available experimental data [68, 69]. As is known, the systematically collected data concerning the most important quadrupole deformation parameter β_2 can be obtained not only from reduced transition probabilities $B(E2)$ [68, 69] but also from experimental quadrupole moment values [69]. The β_2 value given by using the reduced transition probabilities $B(E2)$ is always positive and by definition automatically include the dynamic effect. The quadrupole deformation β_2 calculated from the quadrupole moment values are obtained not considering nuclear surface vibrations since the relationship is obtained by assuming near spherical nucleus shape vibrations amplitude is small in comparison to nucleus equilibrium deformation.

Note that based on the measured static electric quadrupole moment Q values in the laboratory system [69], the β_2 is calculated by [70]

$$\beta_2 = \frac{15Q}{19Z\langle r \rangle^2} \frac{(I+1)(2I+3)}{3K^2 - I(I+1)}, \quad (8)$$

where I is the spin of the state and K is the angular momentum projection on symmetry axis. Considering the surface diffusion properties in light nuclei (e.g., for $A \leq 100$), the value of $\langle r^2 \rangle$ was evaluated using the expression [71]

$$\langle r^2 \rangle = \frac{0.6R_0^2(1 + 10/3(\pi a_0/R_0)^2)}{1 + (\pi a_0/R_0)^2}, \quad (9)$$

where the parameters $R_0 = 1.07A^{1/3}$ fm and $a_0 = 0.55$ fm (which can be obtained from the data on fast electrons scattering). For $A > 100$, $\langle r^2 \rangle = 0.6 \times (1.2A^{1/3})^2 \text{fm}^2$. Usually, there are rather obvious differences between these two experimental β_2 values extracted from measured $B(E2)$ and Q , especially in the soft nuclei. As we can see from Fig. 3(a), it seems that the difference of β_2 values from two different kinds of measurements supports to consider the vibrating effects in the light nuclei during the calculations. In the heavier nuclei, our calculations agree with the available data and the results given by Möller et al [57]. Moreover, the calculated deformations, e.g., β_2 , are in good agreement with the empirical analysis, e.g., cf. Fig. 2. The γ and β_4 deformations are attracting much interest in the research of nuclear shape as well. The present calculations will provide some useful information but the anomalous points (e.g., the anomalous β_2^Q in $^{170}_{66}\text{Dy}_{94}$, as seen in Fig. 3(a)) will need to verify.

Nuclear stability (or rate of decay), which is governed by a combination of quantum mechanical rules, nuclear forces, and electrostatic charge, is usually measured in terms of half-life. In Fig. 4, we present the half-lives of 59 isotopic chains, from $Z = 2$ to 118, taking the selected nuclei on the β -stability line as footholds. That is, the

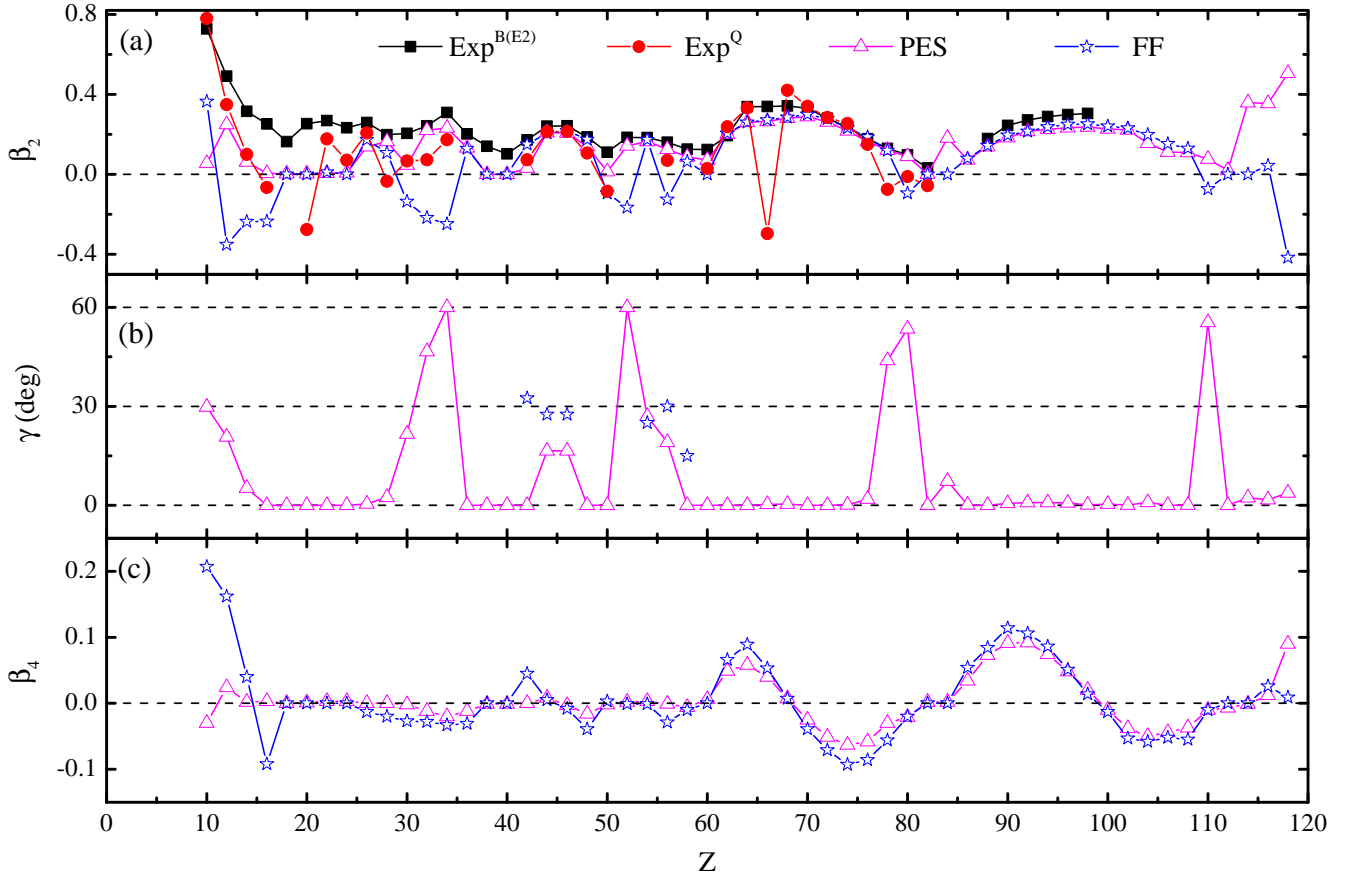


FIG. 3. (Color online) Calculated ground-state equilibrium deformations (a) β_2 , (b) γ and (c) β_4 for even-even nuclei with $10 \leq Z \leq 118$ along the β -stability line, compared with the FY+FRDM (FF) calculations [57] and the available data [68, 69]. Note that the selected nucleus (e.g., N or A) for a given Z is determined by the Green's expression [3], $N - Z = 0.4A^2/(A+200)$, and two PES calculations give the same equilibrium deformations. See the text for more details.

half-lives are plotted against N but the corresponding N of nuclei on the stability line are used for the reference coordinates. After such coordinate shifts, one can easily find that the half-lives in each isotopic chain systematically decrease as the neutron number N moves away from the reference point at least up to the Pb isotopes. Above $Z = 82$, it seems that the half-life properties lose the systematic behaviour visible for the lighter nuclei. From the present data with $Z > 82$, regardless of the N number, no stable nuclei exist except for several so-called primordial radioactive nuclides (e.g., ^{232}Th , $^{235,238}\text{U}$ and ^{244}Pu).

Moreover, one can notice that two maxima may appear during the half-life evolution though both are unstable. In addition, it is found that below the $Z = 50$ Sn isotopes there are more data on the right side of the stability line while after this isotopes more data are observed on the neutron-deficient side. In particular, all the observed data locate on the left side of the stability line, namely the neutron-deficient direction. To explore along the stability line, the neutron-rich projectile-target combinations seem necessary. Note that the $^{294}_{118}\text{Os}_{176}$ nucleus with the largest Z up to now has been identified but there

is neither half-life information available nor two-nucleon separation energies. It is certainly expected that the half-lives will rapidly increase as approaching the $^{298}_{114}\text{Fl}_{184}$ nucleus, verifying the prediction of the 'island of stability'. Anyway, from the new angle of view (standing on the β -stability line), it seems that one can easily notice some systematic properties which may be helpful for deducing the related physics behind them.

The binding energy and the nucleon(s) separation energy are of importance for nuclear structure. They can provide important information on the relative stability of nuclei, the nucleon-nucleon interactions in the nucleus, the bound limits of nuclei, the shell gaps, and so on. [72]. Under the same horizontal-coordinate convention to Figure. 4, Figure 5 illustrates the available two-nucleon separation energies for 59 even-even isotopic chains. As is well known, separation energies of isotopic (isotonic) nuclei of a given parity type (e.g., even-even, even-odd, odd-even, or odd-odd) follow linear systematics within each shell region if plotted in a function of N (Z) [10]. Indeed, as seen in Fig. 5, one can see such linear systematics: the two-neutron separation energy generally decreases with increasing N , reflecting the symmetry en-

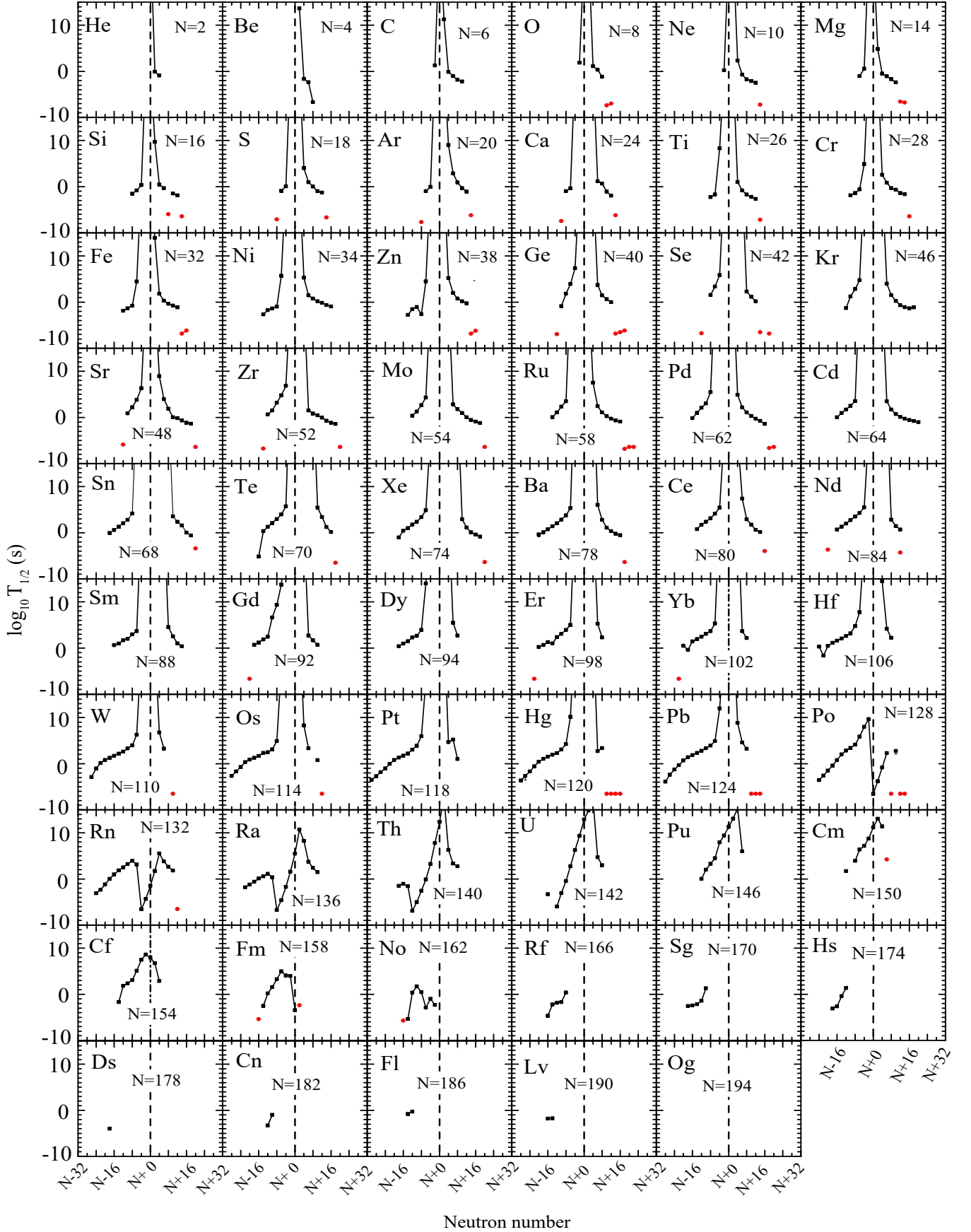


FIG. 4. (Color online) The experimental half-lives (in \log_{10} -scale) of even-even nuclei along 59 different isotopic chains, for each subfigure, taking the corresponding neutron number N (cf. the dash line and the N number given for each isotopic chain) of the even-even nucleus on the β -stability line as a reference. The data are taken from the Ref. [25] and the red solid circle denotes the lower limit of data (e.g., for ^{140}Te $T_{1/2} > 300$ ns, the data 300 ns is adopted).

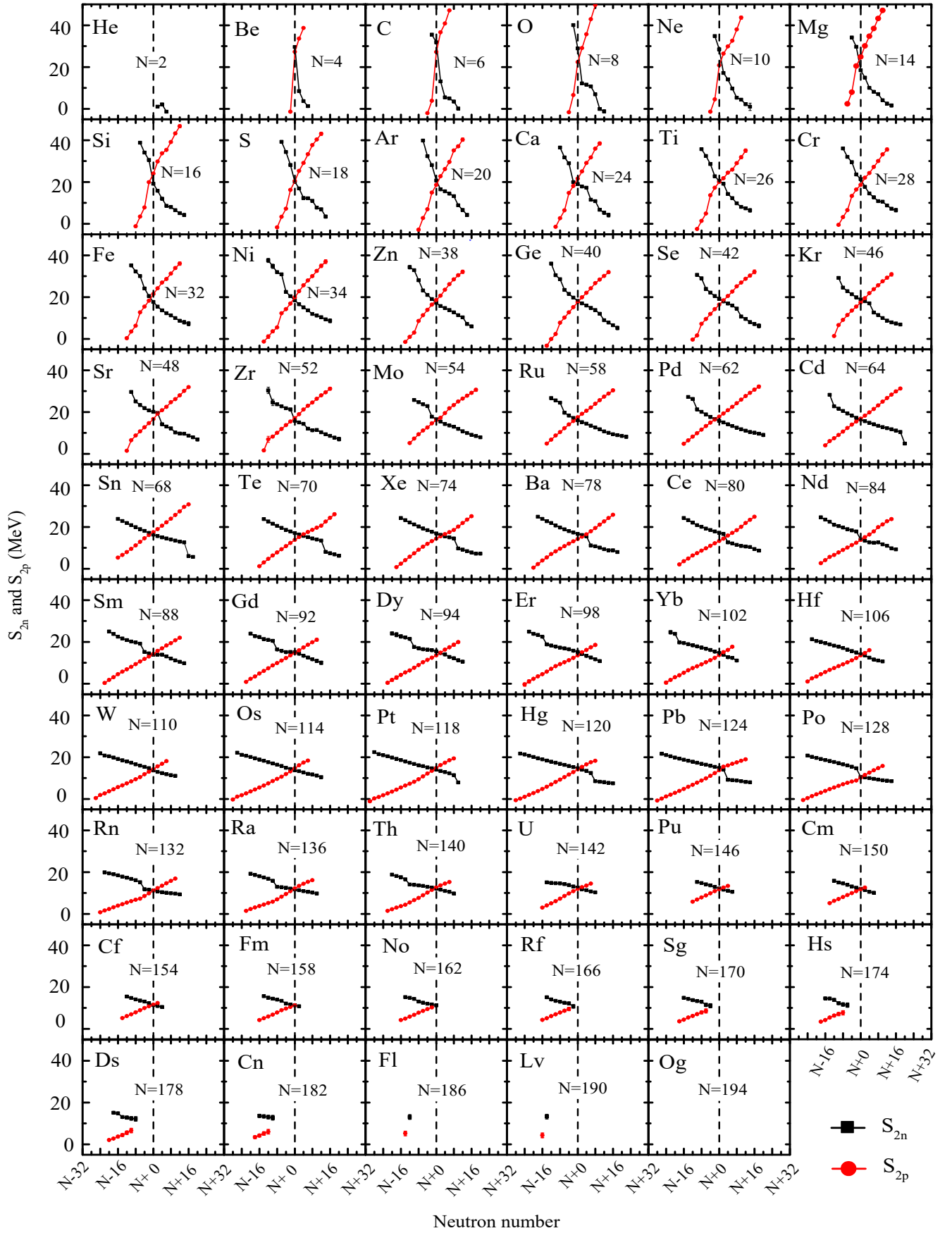


FIG. 5. (Color online) Similar to Fig. 4, but for two-proton and two-neutron separation energies. The data are taken from the Ref. [10].

ergy and the shell filling, while at certain values of N the slope of the curve changes sharply [72], corresponding to the shell closure; the opposite trend for two-proton separation energies. Meanwhile, it can be found from Fig. 5 that two lines for two-proton and two-neutron separation energies in each isotopic chain cross at the stability line and the absolute values of the slopes of these two lines have a decreasing trend with the increasing proton number Z . Above $^{264}_{102}\text{No}_{162}$, experimental data are scarce but the evolution trends seem to be valid and await experimental clarification.

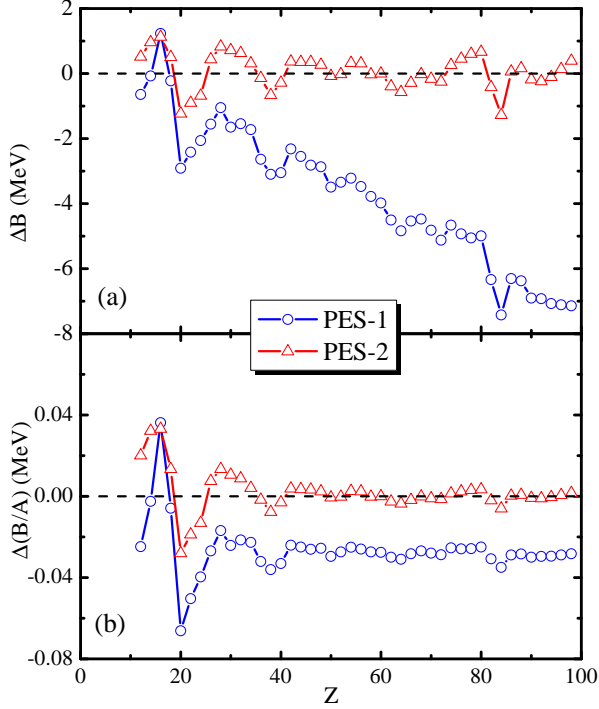


FIG. 6. (Color online) Comparison of discrepancies between experimental and calculated (a) binding energies and (b) binding energy per nucleon based on the first (PES-1) and the second (PES-2) methods (e.g., see the text for more details) for even-even nuclei along the β -stability line. Proton number 12 is the lowest value of Z that we consider in the present investigation. Experimental data are from Ref. [10].

Figure 6 shows the comparison of discrepancies between experimental and calculated binding energy and binding energy per nucleon based on two PES methods for even-even nuclei along the β -stability line. The discrepancies of binding energy and binding energy per nucleon are defined as $\Delta B = B^{\text{exp.}}(Z, N) - B^{\text{theo.}}(Z, N)$ and $\Delta B/A = B^{\text{exp.}}(Z, N)/A - B^{\text{theo.}}(Z, N)/A$, respectively. Obviously, one can notice that the improved method gives better agreement with experimental data, especially for nuclei above $N = 40$. The improvement in the second method reduced the root mean square error in the calculated binding energies from 4.305 MeV to 0.533 MeV and the error in the calculated binding energies per nucleon from 0.030 MeV to 0.010 MeV.

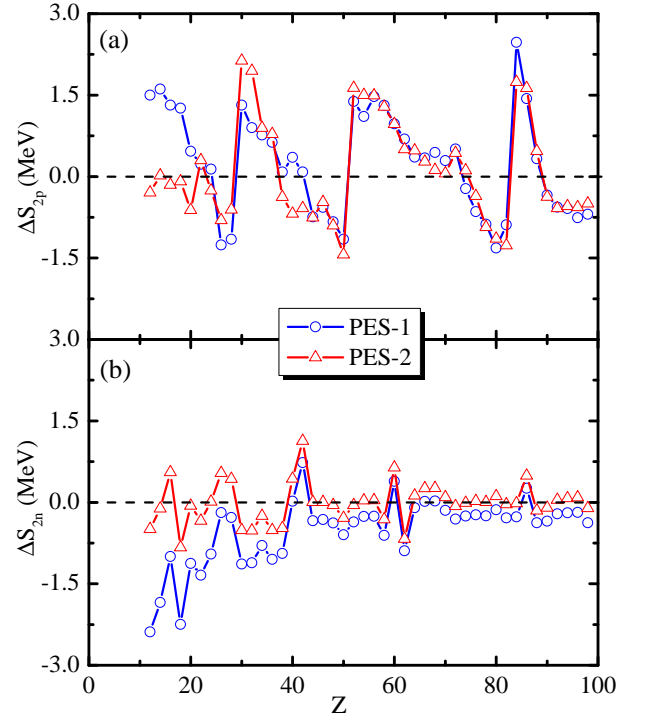


FIG. 7. (Color online) Similar to Fig. 6, but for (a) two-proton separation energies S_{2p} and (b) two-neutron separation energies S_{2n} . Data are taken from Ref. [10].

Figure 7 shows the discrepancies between experimental and calculated two-nucleon separation energies, e.g., defined by $\Delta S_{2n} = S_{2n}^{\text{exp.}}(Z, N) - S_{2n}^{\text{theo.}}(Z, N)$ for neutrons and $S_{2n}(Z, N) = B(Z, N) - B(Z, N - 2)$ (similarly, for protons). It should be pointed out that we take the convention that binding energy $B(Z, N)$ is positive. As seen in Fig. 7(a), the differences ΔS_{2p} have a complicated zigzag pattern in these two calculated results. This behaviour may be due to the presence of large shell effects at proton closures which lead to jump in the binding energy. However, it is interesting that such behaviour seems not to occur for neutrons, as seen in Fig. 7(b). One can find that the discrepancies between theory and experiment have a decreasing trend with increasing Z . The improvement in the second method reduced the root mean square error in the calculated two-proton separation energies from 0.966 MeV to 0.926 MeV and the error in the calculated two-neutron separation energies from 0.802 MeV to 0.368 MeV.

Based on the improved PES method, Figure 8 shows the calculated two-proton and two-neutron separation energies for even-even nuclei up to the predicted superheavy island along the stability line and their differences, together with the comparison with experiments. It seems that the two-neutron separation energies against Z represent an approximately linear relationship, decreasing with increasing proton numbers. It is known that two-neutron separation energies approximately equal twice the chemical potential λ . As illustrated in Fig. 8(a),

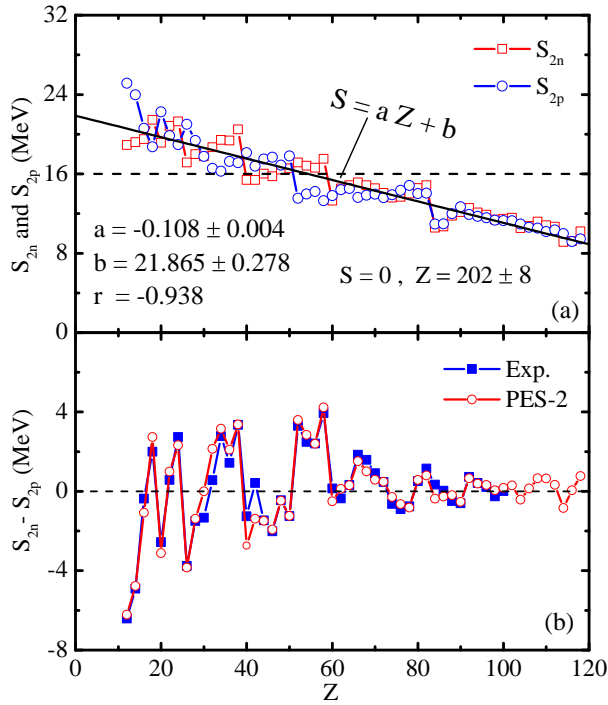


FIG. 8. (Color online) (a) Calculated two-nucleon separation energies S_{2p} (circles) and S_{2n} (squares) of even-even nuclei along the stability line against Z up to 118 in terms of the second PES method; the results of the linear least-square fit are also shown, where r is the Pearson correlation coefficient. (b) Comparison of differences between experimental (solid squares) and calculated (using the improved PES method, cf. open circle symbols) values of $S_{2n} - S_{2p}$. Data are taken from Ref. [10].

the two-nucleon separation energies are still more than 8 MeV for the nuclei up to $Z = 118$ on the stability line, indicating that the nucleons will be strongly bound at these zones. Based on a simple linear least-square fit, we can crudely estimate the bound limit (e.g., when $S = 0$, $Z = 202 \pm 8$) along the stability line. Combining the formula of the β -stability line, it is easy to determine that the heaviest even-even bound nucleus may be (or be close to) the $^{574}_{372}202$ nucleus (between $^{548}_{354}194$ and $^{600}_{390}210$ along the stability line). From Fig. 8(b), one can see that both theoretically and experimentally, the differences between S_{2n} and S_{2p} exhibit an obvious staggering behavior but the calculated results agree with available data very well,

which will indicate the extrapolations to high Z region along the stability line are reasonable and believable to an extent using the improved PES method. Practically, this bound limit is almost impossible to be verified nowadays. However, it still bears some information in theoretical point of view.

IV. SUMMARY

In summary, we have systematically investigated the evolution of structural properties along the β -stability line based on the PES method in the $(\beta_2, \gamma, \beta_4)$ deformation space. The predicted nuclear mass (binding energy), which is a critical input quantity for nuclear reaction and decay, is to an extent improved by using the new modeling and parameters for macroscopic energy. We compared the calculated ground-state deformations with experiments and the previous theoretical results. It seems that the vibrational effect may not be ignored and responsible for the deformation disagreement between experiment and theory in the soft nuclei. Taking the nucleus on the stability line as origin of coordinate, one can see the very similar signatures of the evolution both for two-nucleon separation energies and for nuclear half lives in its isotopic and isotonic chains. The binding energy and two-nucleon separation energy of the nuclei on the β -stability line are investigated and analyzed, indicating the improved PES calculations can describe experimental data better. Further, we crudely estimate the bound limit along the stability line. The present investigation will be helpful for systematically understanding the structure evolution of nuclei along the stability line, up to the predicted superheavy island. It will also be interesting to further examine their related properties at, e.g., high-spin and/or high-temperature (excitation energy) conditions in the future.

ACKNOWLEDGMENTS

This work was supported by the National Natural Science Foundation of China (Nos. 11975209, U2032211 and 12075287), the Physics Research and Development Program of Zhengzhou University (No. 32410017), the Project of Youth Backbone Teachers of Colleges and Universities of Henan Province (No. 2017GGJS008) and the Polish National Science Centre under Contract No. 2016/21/B/ST2/01227. Some of the calculations were conducted at the National Supercomputing Center in Zhengzhou.

- [1] J. Erler, N. Birge, M. Kortelainen, W. Nazarewicz, E. Olsen, A. M. Perhac, and M. Stoitsov, The limits of the nuclear landscape, *Nature* **486**, 509 (2012).
- [2] I. Tanihata, Radioactive beam science, past, present and future, *Nucl. Instrum Methods B* **266**, 4067 (2008).

- [3] A. E. S. Green, *Nuclear Physics* (McGraw-Hill Book Company, Inc., New York, 1955) p.250.
- [4] P. Marmier and E. Sheldon, *Physics of nuclei and particles*, (Academic Press, New York, 1971).

- [5] M. G. Mayer, On closed shells in nuclei. II, *Phys. Rev.* **75**, 1969 (1949).
- [6] M. G. Mayer, Nuclear configurations in the spin-orbit coupling model. I. Empirical Evidence, *Phys. Rev.* **78**, 16 (1950).
- [7] O. Haxel, J. Hans. D. Jensen, and H. E. Suess, On the “magic numbers” in nuclear structure, *Phys. Rev.* **75**, 1766 (1949).
- [8] D. Haxel, J. H. D. Jensen, and H. E. Suess, Modellmäßige Deutung der ausgezeichneten Nukleonenzahlen im Kernbau, *Z. Phys.* **128**, 295 (1950).
- [9] K. Heyde, Basic Ideas and Concepts in Nuclear Physics, 2nd ed. (IOP Publishing, Bristol, 1999).
- [10] M. Wang, G. Audi, F. G. Kondev, W. J. Huang, S. Naimi, and X. Xu, The AME2016 atomic mass evaluation (II). Tables, graphs and references, *Chin. Phys. C* **41**, 030003 (2017).
- [11] U. Mosel and W. Greiner, On the stability of superheavy nuclei against fission, *Z. Phys.* **222**, 261 (1969).
- [12] S. Nilsson, C. Tsang, A. Sobieczewski, Z. Szymański, S. Wycech, C. Gustafson, I. L. Lamm, P. Möller, and B. Nilsson, On the nuclear structure and stability of heavy and superheavy elements, *Nucl. Phys. A* **131**, 1 (1969).
- [13] Z. Patyk and A. Sobieczewski, Ground-state properties of the heaviest nuclei analyzed in a multidimensional deformation space, *Nucl. Phys. A* **533**, 132 (1991).
- [14] P. Möller and J. R. Nix, Stability of heavy and superheavy elements, *J. Phys. G* **20**, 1681 (1994).
- [15] R. Smolańczuk, Properties of the hypothetical spherical superheavy nuclei, *Phys. Rev. C* **56**, 812 (1997).
- [16] P. Möller, J. R. Nix, and K.-L. Kratz, Nuclear properties for astrophysical and radioactive-ion-beam applications, *At. Data Nucl. Data Tables* **66**, 131 (1997).
- [17] S. G. Nilsson, S. G. Thompson, and C. F. Tsang, Stability of superheavy nuclei and their possible occurrence in nature, *Phys. Lett.* **28B**, 458 (1969).
- [18] P. Möller, J. R. Nix, W. D. Myers, and W. J. Swiatecki, Nuclear ground-state and deformations, *At. Data Nucl. Data Tables* **59**, 185 (1995).
- [19] A. Mamdouh, J. M. Pearson, M. Rayet, and F. Tondeur, Fission barriers of neutron-rich and superheavy nuclei calculated with the ETFSI method, *Nucl. Phys. A* **679**, 337 (2001).
- [20] S. Ćwiok, J. Dobaczewski, P. H. Heenen, P. Magierski, and W. Nazarewicz, Shell structure of the superheavy elements, *Nucl. Phys. A* **611**, 211 (1996).
- [21] K. Rutz, M. Bender, T. Bürvenich, T. Schilling, P.-G. Reinhard, J. A. Maruhn, and W. Greiner, Superheavy nuclei in self-consistent nuclear calculations, *Phys. Rev. C* **56**, 238 (1997).
- [22] M. Bender, K. Rutz, P.-G. Reinhard, J. A. Maruhn, and W. Greiner, Shell structure of superheavy nuclei in self-consistent mean-field models, *Phys. Rev. C* **60**, 034304 (1999).
- [23] G. A. Lalazissis, M. M. Sharma, P. Ring, and Y. K. Gambhir, Superheavy nuclei in the relativistic mean-field theory, *Nucl. Phys. A* **608**, 202 (1996).
- [24] Yu. Ts. Oganessian, A. V. Yeremin, A. G. Popeko, S. L. Bogomolov, G. V. Buklanov, M. L. Chelnokov, V. I. Chepigin, B. N. Gikal, V. A. Gorshkov, G. G. Gulbekian, M. G. Itkis, A. P. Kabachenko, A. Yu. Lavrentev, O. N. Malyshev, J. Rohac, R. N. Sagaidak, S. Hofmann, S. Saro, G. Giardina, and K. Morita, Synthesis of nuclei of the superheavy element 114 in reactions induced by ^{48}Ca , *Nature (London)* **400**, 242 (1999).
- [25] National Nuclear Data Center. Evaluated Nuclear Structure Data File <http://www.nndc.bnl.gov/ensdf/>.
- [26] Here we adopt the suggested IUPAC name for element 118, Oganesson. See <http://iupac.org/>.
- [27] P. Schwerdtfeger, Toward an accurate description of solid-state properties of superheavy elements—A case study for the element Og ($Z = 118$), *EPJ Web Conf.* **131**, 07004 (2016).
- [28] S. Hofmann and G. Münzenberg, The discovery of the heaviest elements, *Rev. Mod. Phys.* **72**, 733 (2000).
- [29] Y. Oganessian, Heaviest nuclei from ^{48}Ca -induced reactions, *J. Phys. G: Nucl. Part. Phys.* **34**, R165 (2007).
- [30] H. L. Wang, J. Yang, M. L. Liu, and F. R. Xu, Evolution of ground-state quadrupole and octupole stiffnesses in even-even barium isotopes, *Phys. Rev. C* **92**, 024303 (2015).
- [31] H. L. Wang, S. Zhang, M. L. Liu, and F. R. Xu, Nuclear stiffness evolutions against axial and non-axial quadrupole deformations in even- A osmium isotopes, *Prog. Theor. Exp. Phys.*, 073D03 (2015).
- [32] Q. Yang, H. L. Wang, M. L. Liu, and F. R. Xu, Characteristics of collectivity along the yrast line in even-even tungsten isotopes, *Phys. Rev. C* **94**, 024310 (2016).
- [33] Q. Z. Chai, W. J. Zhao, M. L. Liu, and H. L. Wang, Calculation of multidimensional potential energy surfaces for even-even transuranium nuclei: systematic investigation of the triaxiality effect on the fission barrier, *Chin. Phys. C* **42**, 054101 (2018).
- [34] H. Y. Meng, Y. W. Hao, H. L. Wang, and M. L. Liu, Signature of yrast-state structure in even-even hafnium isotopes based on traditional total-Routhian-surface calculations and novel E-GOS curves, *Prog. Theor. Exp. Phys.* 103D02 (2018).
- [35] Q. Z. Chai, W. J. Zhao, and H. L. Wang, Effects of various deformation on the first fission barrier in even- A $N = 152$ isotones, *Commun. Theor. Phys.* **71**, 67 (2019).
- [36] Z. Z. Zhang, H. L. Wang, H. Y. Meng, and M. L. Liu, Uncertainty evaluation and correlation analysis of single-particle energies in phenomenological nuclear mean field: an investigation into propagating uncertainties for independent model parameters, *Nucl. Sci. Tech.* **32**, 16 (2021).
- [37] J. R. Nix, Calculation of fission barriers for heavy and superheavy nuclei, *Annu. Rev. Nucl. Sci.* **22**, 65 (1972).
- [38] S. Ćwiok, J. Dudek, W. Nazarewicz, J. Skalski, and T. Werner, Single-particle energies, wave functions, quadrupole moments and g -factors in an axially deformed Woods-Saxon potential with applications to the two-centre-type nuclear problems, *Comp. Phys. Comm.* **46**, 379 (1987).
- [39] V. M. Strutinsky, Shell effects in nuclear masses and deformation energies, *Nucl. Phys. A* **95**, 420 (1967).
- [40] H. C. Pradhan, Y. Nogami, and J. Law, Study of approximations in the nuclear pairing-force problem, *Nucl. Phys. A* **201**, 357 (1973).
- [41] P. Möller and J. R. Nix, Nuclear pairing models, *Nucl. Phys. A* **536**, 20 (1992).
- [42] W. D. Myers and W. J. Swiatecki, Nuclear masses and deformations, *Nucl. Phys. A* **81**, 1 (1966).
- [43] P. Möller, W. D. Myers, W. J. Swiatecki, and J. Treiner, Nuclear mass formula with a finite-range droplet model

- and a folded-Yukawa single-particle potential, *At. Data Nucl. Data Tables* **39**, 225 (1988).
- [44] K. Pomorski and J. Dudek, Nuclear liquid-drop model and surface-curvature effects, *Phys. Rev. C* **67**, 044316 (2003).
- [45] A. Bhagwat, X. Viñas, M. Centelles, P. Schuck, and R. Wyss, Microscopic-macroscopic approach for binding energies with the Wigner-Kirkwood method, *Phys. Rev. C* **81**, 044321 (2010).
- [46] Z. Y. Wu, C. Qi, R. Wyss, and H. L. Liu, Global calculations of microscopic energies and nuclear deformations: Isospin dependence of the spin-orbit coupling, *Phys. Rev. C* **92**, 024306 (2015).
- [47] M. Bolsterli, E. O. Fiset, J. R. Nix, and J. L. Norton, New calculation of fission barriers for heavy and superheavy nuclei, *Phys. Rev. C* **5**, 1050 (1972).
- [48] F. R. Xu, P. M. Walker, J. A. Sheikh, and R. Wyss, Multi-quasiparticle potential-energy surfaces *Phys. Lett. B* **435**, 257 (1998).
- [49] R. F. Casten, D. S. Brenner, and P. E. Haustein, Valence $p - n$ interactions and the development of collectivity in heavy nuclei, *Phys. Rev. Lett.* **58**, 658 (1987).
- [50] R. F. Casten, Possible unified interpretation of heavy nuclei, *Phys. Rev. Lett.* **54**, 1991 (1985).
- [51] R. F. Casten, $N_p N_n$ Systematics in heavy nuclei, *Nucl. Phys. A* **443**, 1 (1985).
- [52] R. F. Casten and N. V. Zamfir, The evolution of nuclear structure: the $N_p N_n$ scheme and related correlations, *J. Phys. G: Nucl. Part. Phys.* **22**, 1521 (1996).
- [53] N. Fouladi, J. Fouladi, and H. Sabri, Investigation of low-lying energy spectra for deformed prolate nuclei via partial dynamical $SU(3)$ symmetry, *Eur. Phys. J. Plus* **130**, 112 (2015).
- [54] P. Reiter, T. L. Khoo, C. J. Lister, D. Seweryniak, I. Ahmad, M. Alcorta, M. P. Carpenter, J. A. Cizewski, C. N. Davids, G. Gervais, J. P. Greene, W. F. Henning, R. V. F. Janssens, T. Lauritsen, S. Siem, A. A. Sonzogni, D. Sullivan, J. Uusitalo, I. Wiedenhöver, N. Amzal, P. A. Butler, A. J. Chewter, K. Y. Ding, N. Fotiadis, J. D. Fox, P. T. Greenlees, R.-D. Herzberg, G. D. Jones, W. Korten, M. Leino, and K. Vetter, Ground-state band and deformation of the $Z = 102$ isotope ^{254}No , *Phys. Rev. Lett.* **82**, 509 (1999).
- [55] P. T. Greenlees, J. Rubert, J. Piot, B. J. P. Gall, L. L. Andersson, M. Asai, Z. Asfari, D. M. Cox, F. Dechery, O. Dorvaux, T. Grahm, K. Hauschild, G. Henning, A. Herzan, R.-D. Herzberg, F. P. Heßberger, U. Jakobsson, P. Jones, R. Julin, S. Juutinen, S. Ketelhut, T.-L. Khoo, M. Leino, J. Ljungvall, A. Lopez-Martens, R. Lozeva, P. Nieminen, J. Pakarinen, P. Papadakis, E. Parr, P. Peura, P. Rahkila, S. Rinta-Antila, P. Ruotsalainen, M. Sandzelius, J. Sarén, C. Scholey, D. Seweryniak, J. Sorri, B. Sulignano, Ch. Theisen, J. Uusitalo, and M. Venhart, Shell-structure and pairing interaction in superheavy nuclei: Rotational properties of the $Z = 104$ nucleus ^{256}Rf , *Phys. Rev. Lett.* **109**, 012501 (2012).
- [56] H. L. Wang, Q. Z. Chai, J. G. Jiang, and M. L. Liu, Rotational properties in even-even superheavy $^{254-258}\text{Rf}$ nuclei based on total-Routhian-surface calculations, *Chin. Phys. C* **38**, 074101 (2014).
- [57] P. Möller, A. J. Sierk, T. Ichikawa and H. Sagawa, Nuclear ground-state masses and deformations: FRDM(2012), *At. Data Nucl. Data Tables* (2016).
- [58] C. A. Mallmann, System of levels in even-even nuclear, *Phys. Rev. Lett.* **2**, 507 (1959).
- [59] F. Iachello, Analytic description of critical point nuclei in a spherical-axially deformed shape phase transition, *Phys. Rev. Lett.* **87**, 052502 (2001).
- [60] J. B. Gupta, New perspective in rotation vibration interaction, *Int. J. Mod. Phys. E* **22**, 1350023 (2013).
- [61] D. Bonatsos, D. Lenis, N. Minkov, D. Petrellis, P.P. Raychev, and P.A. Terziev, Ground state bands of the $E(5)$ and $X(5)$ critical symmetries obtained from Davidson potentials through a variational procedure, *Phys. Lett. B* **584**, 40 (2004).
- [62] D. Bonatsos, D. Lenis, D. Petrellis, and P. A. Terziev, $Z(5)$: critical point symmetry for the prolate to oblate nuclear shape phase transition, *Phys. Lett. B* **588**, 172 (2004).
- [63] F. Iachello, Dynamic symmetries at the critical point, *Phys. Rev. Lett.* **85**, 3580 (2000).
- [64] F. Iachello, N. V. Zamfir, and R. F. Casten, Phase coexistence in transitional nuclei and the Interacting-Boson Model, *Phys. Rev. Lett.* **81**, 1191 (1998).
- [65] R. F. Casten, D. Kusnezov, and N. V. Zamfir, Phase transitions in finite nuclei and the integer nucleon number problem, *Phys. Rev. Lett.* **82**, 5000 (1999).
- [66] A. S. Davydov and G. F. Filippov, Rotational states in even atomic nuclei, *Nucl. Phys.* **8**, 237 (1958).
- [67] R. F. Casten, Shape phase transitions and critical-point phenomena in atomic nuclei, *Nat. Phys.* **2**, 811 (2006).
- [68] S. Raman, C. W. Nestor Jr., and P. Tikkanen, Transition probability from the ground to the first-excited 2^+ state of even-even nuclides, *At. Data Nucl. Data Tables* **78**, 1 (2001).
- [69] N. J. Stone, Table of nuclear magnetic dipole and electric quadrupole moments, *At. Data Nucl. Data Tables* **90**, 75 (2005).
- [70] I. M. Kapitonov, Introduction into Nuclei and Particles Physics (Editorial Urss, Moscow, 2002).
- [71] I. Boboshin, B. Ishkhanov, S. Komarov, V. Orlin, N. Peskov, and V. Varlamov, Investigation of quadrupole deformation of nucleus and its surface dynamic vibrations, *Int. Conf. Nucl. Data for Sci. and Tech.* **65**, (2007).
- [72] A. Gelberg, H. Sakurai, M. W. Kirson, and S. Heinze, Wigner energy and shell gaps in two-nucleon separation energies, *Phys. Rev. C* **80**, 024307 (2009).